

Spatial Distribution of PEO–PPO–PEO Block Copolymer and PEO Homopolymer in Lipid Bilayers

Mihee Kim, Frank Heinrich, Greg Haugstad,* Guichuan Yu, Guangcui Yuan, Sushil K. Satija, Wenjia Zhang, Hannah S. Seo, Joseph M. Metzger, Samira M. Azarin, Timothy P. Lodge, Benjamin J. Hackel, and Frank S. Bates*



Cite This: *Langmuir* 2020, 36, 3393–3403



Read Online

ACCESS |



Metrics & More

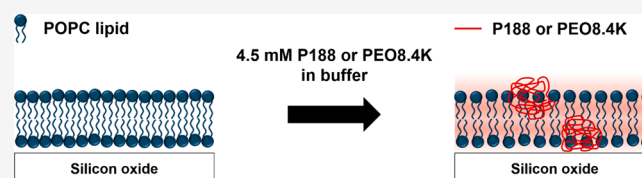


Article Recommendations



Supporting Information

ABSTRACT: Maintaining the integrity of cell membranes is indispensable for cellular viability. Poloxamer 188 (P188), a poly(ethylene oxide)-*b*-poly(propylene oxide)-*b*-poly(ethylene oxide) (PEO–PPO–PEO) triblock copolymer with a number-average molecular weight of 8700 g/mol and containing 80% by mass PEO, protects cell membranes from various external injuries and has the potential to be used as a therapeutic agent in diverse applications. The membrane protection mechanism associated with P188 is intimately connected with how this block copolymer interacts with the lipid bilayer, the main component of a cell membrane. Here, we report the distribution of P188 in a model lipid bilayer comprising 1-palmitoyl-2-oleoyl-glycero-3-phosphocholine (POPC) using neutron reflectivity (NR) and atomic force microscopy (AFM). We also investigated the association of a PEO homopolymer (PEO8.4K; $M_n = 8400$ g/mol) that does not protect living cell membranes. These experiments were conducted following incubation of a 4.5 mmol/L polymer solution in a buffer that mimics physiological conditions with supported POPC bilayer membranes followed by washing with the aqueous medium. In contrast to previous reports, which dealt with P188 and PEO in salt-free solutions, both P188 and PEO8.4K penetrate into the inner portion of the lipid bilayer as revealed by NR, with approximately 30% by volume occupancy across the membrane without loss of bilayer structural integrity. These results indicate that PEO is the chemical moiety that principally drives P188 binding to bilayer membranes. No defects or phase-separated domains were observed in either P188- or PEO8.4K-incubated lipid bilayers when examined by AFM, indicating that polymer chains mingle homogeneously with lipid molecules in the bilayer. Remarkably, the breakthrough force required for penetration of the AFM tip through the bilayer membrane is unaffected by the presence of the large amount of P188 and PEO8.4K.



INTRODUCTION

The cell plasma membrane is a semipermeable barrier that protects intracellular components and regulates transport. Disruption of the cell membrane is common under physiological duress, particularly in cardiac/skeletal muscles where high mechanical stress is imposed.¹ If the cell membrane is not properly protected or repaired, biological functions are compromised due to increased permeability, which can lead to cell death. The first synthetic polymer identified to be capable of protecting the cell membrane is Poloxamer 188 (P188; also known as Pluronic F68).² P188 is a nonionic triblock copolymer composed of a central poly(propylene oxide) (PPO) block flanked by two poly(ethylene oxide) (PEO) blocks with 80% by mass PEO (Figure 1a). P188 has exhibited cell membrane protection against many different types of injuries including osmotic,³ oxidative,⁴ and shear stress⁵ as well as electrical⁶ and heat shocks⁷ for various cell types such as endothelial cells,⁸ epithelial cells,⁹ neurons,¹⁰ cardiac¹¹ and skeletal muscle cells,¹² and fibroblasts.⁷ P188 successfully restored muscle cell membrane integrity in models of Duchenne muscular dystrophy,^{11,13–15} a fatal disease known

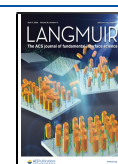
for progressively deteriorating muscles. Also, P188 prevented myocardial ischemia/reperfusion injury, a leading cause of death in patients with cardiovascular disease, through membrane stabilization.^{16–18}

Although *in vivo* and *in vitro* studies with multiple cell types demonstrated the potential of P188 as a universal therapeutic agent for membrane protection, the mechanism of action for P188 to protect or even interact with the cell membrane remains largely unknown. A potential key factor of the protection mechanism is the distribution of polymer chains within the lipid bilayer, which can provide insight into how P188 confers resistance to the bilayer from being ruptured. As a major component of the cell membrane, a phospholipid bilayer is often used as a model membrane system when

Received: October 15, 2019

Revised: March 19, 2020

Published: March 27, 2020



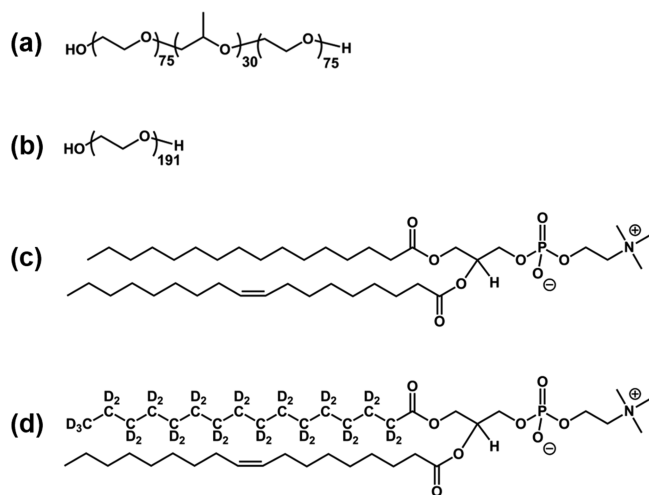


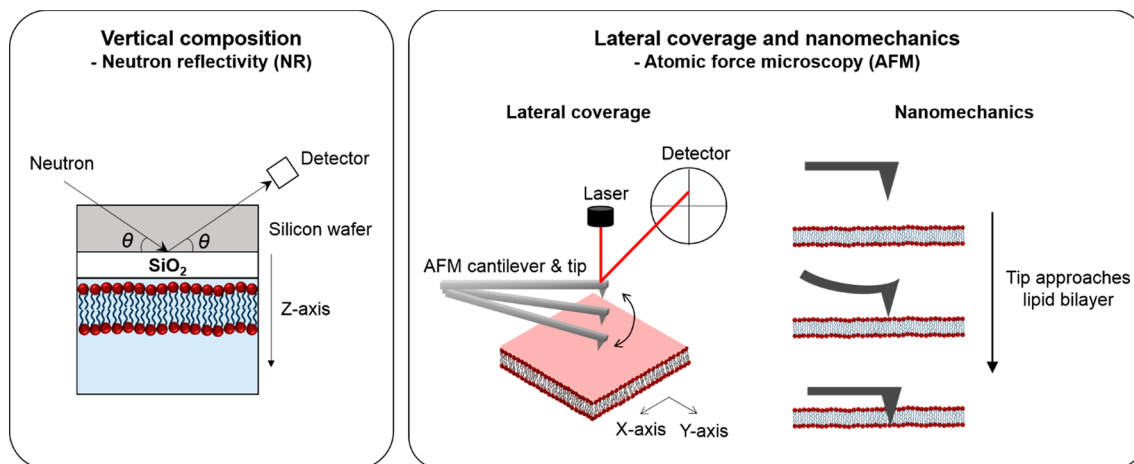
Figure 1. Chemical structures of (a) P188, (b) PEO8.4K, (c) POPC, and (d) tail-deuterated POPC.

studying the consequences of block copolymer–membrane interactions. The insertion depth of P188 into multilamellar lipid vesicles was examined using X-ray scattering.^{19,20} The PPO block of P188 was reported to weakly insert at the interface between the ester linkages and the phosphate headgroups of the lipid. Although this study provided polymer insertion depth depending on PPO or PEO length, the multilamellar vesicles employed in the study were prepared by mixing P188 and lipid molecules before forming bilayers, which does not mimic the physiological circumstance where P188 interacts with an existing (i.e., preformed) single lipid bilayer that makes up a cell membrane. Moreover, the low scattering contrast between P188 and the hydrocarbon lipid tails limited detailed identification of the extent of P188 penetration. ¹H Overhauser dynamic nuclear polarization NMR spectroscopy also has been used to study the location of P188 in large unilamellar vesicles.²¹ Probing local hydration dynamics of water either on the surface or inside the hydrophobic region of the liposome suggested that P188 is weakly adsorbed on the liposome surface without insertion into the membrane at concentrations up to 200 μ M. Neither of these studies identified the lateral distribution of block copolymer along the membrane surface.

In recent work from our group, we employed $M_n = 8600$ g/mol PEO homopolymer ($\bar{D} = 1.06$) as a control in various investigations of the interaction of PEO–PPO–PEO triblock and PEO–PPO diblock copolymers with bilayer vesicles,²² in a cell-based assay³ and with animal models.¹⁴ This PEO homopolymer has a similar molecular weight as P188 ($M_n = 8700$ g/mol) but without a PPO block (Figure 1b) and does not protect cell membranes at the same concentration as P188 in physiological applications.³ The present consensus in the field is that PEO homopolymers do not bind to lipid bilayers, leading to the conjecture that PPO is the critical factor for membrane protection. However, our previous study using surface plasmon resonance spectroscopy revealed that PEO homopolymers also bind to planar lipid bilayers, with similar binding kinetics to that of P188 when exposed to 4.5 mmol/L buffered polymer solutions.²³ This discrepancy between our results and previous studies could be due to different experimental conditions (i.e., salt concentration, incubation time and temperature, polymer concentration, molecular weight of polymers). For example, PEO was dissolved in pure water^{21,24} and incubated for 0 min²¹ or 5 min²⁴ with a lipid bilayer at room temperature.²⁴ Other previous studies used 2000 g/mol PEO grafted onto a lipid bilayer.²⁵ As we aim to elucidate cell membrane protection mechanisms by the polymers, we used a salt concentration that mimics physiological conditions and incubated the polymers in contact with the bilayer at 37 °C for sufficient time to achieve equilibrium adsorption. Our observation that $M_n = 8600$ g/mol PEO homopolymer also binds to a 1-palmitoyl-2-oleoyl-glycero-3-phosphocholine (POPC) lipid bilayer at physiological salt concentration implies that the PEO blocks play a significant role in P188 binding to the lipid bilayer. This is not surprising considering that P188 consists of 80% by mass PEO. Because surface plasmon resonance spectroscopy only detects refractive index changes near the surface, details of the three-dimensional distribution of P188 and PEO homopolymer within the lipid bilayer remained unknown.

Here, we combine neutron reflectivity (NR) and atomic force microscopy (AFM) to investigate P188 and $M_n = 8400$ g/mol PEO homopolymer (PEO8.4K) distribution in a supported lipid bilayer. NR offers a precise method to examine the changes in thickness and the molecular composition profile along the vertical direction of a lipid bilayer upon macromolecular binding.²⁶ AFM is a powerful method to probe

Scheme 1. Experimental Schemes of Neutron Reflectivity and Atomic Force Microscopy



surface morphology and the lateral distribution of macromolecules on the surface.²⁷ The marriage of NR and AFM (Scheme 1) provides a synergy to develop a detailed molecular picture of polymers in three-dimensional space within a lipid bilayer. We find here a striking result that both P188 and PEO8.4K reside mostly within the lipid bilayer, distributed from the outer to the inner lipid headgroup and occupying up to 35% of the total membrane volume, when incubated with 4.5 mmol/L polymer solutions. The surfaces of both the P188- and PEO8.4K-incubated lipid bilayers are smooth and homogeneous, indicating that polymer chains mingle uniformly, at length scales less than about 10 nm, with lipid molecules within the bilayer. These results deepen the understanding of how polymers interact with and protect the cell membrane.

MATERIALS AND METHODS

Materials. P188 was generously provided by BASF (Wyandotte, MI). PEO8.4K and salts for buffer solution (NaCl, KCl, CaCl₂, MgCl₂, and 2-[4-(2-hydroxyethyl)piperazin-1-yl]ethanesulfonic acid (HEPES), purity >99.5%) were purchased from Sigma-Aldrich (St. Louis, MO). D₂O (purity >99.9%) was purchased from Cambridge Isotope Laboratories (Tewksbury, MA). POPC 16:0–18:1 and tail-deuterated POPC 16:0-*d*₃₁-18:1 were purchased from Avanti Polar Lipids (Alabaster, AL). Chemical compositions, molecular weights, and dispersities of P188 and PEO8.4K were determined by ¹H nuclear magnetic resonance spectroscopy and matrix assisted laser desorption/ionization time-of-flight mass spectrometry (Figure S1) as described elsewhere.³ Buffer solutions were prepared by dissolving salts in 100% H₂O, 100% D₂O, or a 66% D₂O/34% H₂O mixture (final concentrations: 140 mmol/L NaCl, 5 mmol/L KCl, 2.5 mmol/L CaCl₂, 2 mmol/L MgCl₂, and 10 mmol/L HEPES, pH 5.4). Note that the changes in structure, hydrolysis rate,²⁸ area compressibility/bending modulus,²⁹ and electrical capacitance³⁰ of phosphatidylcholine lipid bilayers at pH 5.4 vs pH 7 are negligible.

Dynamic Light Scattering. Dynamic light scattering was performed on a Brookhaven BI-200SM instrument (Brookhaven Instruments Corporation, Holtsville, NY) at 90° scattering angle using a 637 nm HeNe laser operating at 20 mW. Polymers dissolved in buffer were filtered (0.2 μm pore diameter) and incubated for 20 min at 37 °C before scattering measurements. Scattering data were collected for 5 min with delay times from 0.3 μs to 4 s. The size distributions were obtained by analyzing correlation functions using the regularized positive exponential sum (REPES) algorithm.³¹

Preparation of Supported Lipid Bilayers. Supported lipid bilayers were prepared using the vesicle rupture method on a silicon oxide surface. Tail-deuterated and normal POPC were used to prepare lipid bilayers for the NR and AFM experiments, respectively. The lipids were dissolved in chloroform (10 mg/mL each) in glass vials. A lipid film was prepared by rotating the glass vial slowly under a mild flow of argon to evaporate chloroform, followed by drying in a desiccator for at least 1 h to remove residual solvent. The lipid film was hydrated by immersion in a 2 mol/L NaCl solution under vigorous stirring. To form lipid vesicles, the hydrated lipid solution was either sonicated until the solution became clear or extruded 49 times at room temperature using an Avanti Mini-Extruder fitted with a polycarbonate filter (50 nm pore diameter). The final concentration of the lipid solution was 5 mg/mL. A silicon oxide layer was formed by immersing a silicon wafer in sulfuric acid for 15 min and rinsing thoroughly with distilled water. The acid-treated silicon wafer was cleaned using a UV/ozone cleaner for 30 min to ensure that the surface was hydrophilic and free of contaminants. The wafer was assembled in a flow cell for NR measurement or in a liquid cell for AFM experiments. The wafer surface was incubated with the vesicles for 1 h at 37 °C, followed by thorough rinsing with water to aid vesicle rupture.

NR Measurements and Analysis. NR measurements were performed at the NG7 reflectometer beamline at the National

Institute of Standards and Technology Center for Neutron Research (Gaithersburg, MD). For all NR measurements, a tail-deuterated 1-palmitoyl-2-oleoyl-glycero-3-phosphocholine lipid (*d*₃₁-POPC) was used to prepare supported lipid bilayers. The silicon substrate was assembled in a flow cell designed to fit the NG7 beamline. The flow cells were maintained at 37 ± 1 °C throughout the experiments using a heating circulator. P188 or PEO8.4K was dissolved in 100% D₂O buffer and filtered (0.2 μm pore diameter). The polymer solutions (4.5 mmol/L) were injected into the flow cell and incubated for 2 h. After rinsing residual polymer, NR was measured in the following order: (1) 100% D₂O buffer, (2) mixture of 66% D₂O and 34% H₂O buffer, (3) 100% D₂O buffer. A flow rate of 150 μL/min was used when rinsing polymers or switching between solutions. All NR curves were recorded for 0 ≤ *q*_z ≤ 0.25 Å⁻¹. Data for each curve were collected for at least 6 h to obtain sufficient neutron counting statistics.

Four NR curves (i.e., neat lipid bilayer in 100%/66% D₂O buffers and polymer-incubated lipid bilayer in the same set of two buffers) were simultaneously fitted. Since the traditional slab model³² is impractical to fit spatially intermixing submolecular groups (e.g., polymer chains penetrating the lipid bilayer) along the vertical direction, we used a continuous distribution model.³³ In this model, the lipid bilayer along the vertical (*z*) direction of the membrane was defined with several submolecular groups representing the substrate-proximal and substrate-distal lipid head groups, and substrate-proximal and substrate-distal lipid tails. The thickness of the inner and the outer lipid leaflet of the bilayer were constrained to be the same. Since the headgroup thickness is smaller than what can be resolved by the neutron reflectivity measurement, the thickness of the lipid headgroup distribution was fixed at 9.56 Å, which was obtained from previous NR experiments and MD simulations.³³ A Hermite spline was used to parametrize volume occupancy profiles of polymers without any assumption. When polymers penetrate into the hydrocarbon lipid tail regions, the polymers were modeled to replace lipid material to meet the area confinement. Also, headgroup material was removed proportionally to the amount of replaced hydrocarbon lipid tail per leaflet. This ensures that the ratio of the hydrocarbon and headgroup volume per leaflet remains at a value in agreement with the lipid structure. The spline was defined by six control points that are on average 15 Å apart. Semi-infinite silicon and solvent layers were defined as slabs. Fit parameters were the thickness and scattering length density of the silicon oxide, the distance of the lipid bilayer from the solid support, the bilayer leaflet hydrocarbon thickness, the bilayer surface coverage (i.e., completeness), and the polymer volume surface density and deviation from equidistant spacing associated with every control point of the Hermite spline.³³ A global fit parameter of roughness was applied to all substrate interfaces. An unbiased determination of modeling uncertainties—a necessity for free-form modeling due to the inherent risk of over parametrization—was carried out using a Monte Carlo Markov chain optimizer.³⁴

AFM Measurements. AFM measurements were performed in a buffer with 100% H₂O using a tip-scanned Keysight 5500 SPM instrument. A Keysight 9524B XYZ piezoscanner (≈90 μm lateral range) was operated in open loop for minimal noise imaging and force-versus-*Z* scanner displacement measurements. Polymers were incubated with the lipid bilayer at 37 °C for 2 h, followed by rinsing residual polymers slowly, and then were measured at room temperature. Three aluminum back-coated silicon cantilevers (resonance frequencies of 38.32, 61.49, and 38.33 kHz) with integrated silicon tips (MicroMasch type NSC36) were cleaned using a UV/ozone cleaner (Hitachi High Technologies, Schaumburg, IL) for 5 min immediately before the measurement. The nominal spring constant of the cantilevers was 0.6 N/m, and the nominal radius of curvature of the tips was 8 nm. For reported force measurements the spring constant was calibrated using a commercial hardware/software implementation (Intermodulation Products AB) of the combined Sader and thermal noise methods.³⁵ The spring constants of the cantilevers used for the measurements were 0.62 and 0.59 N/m.

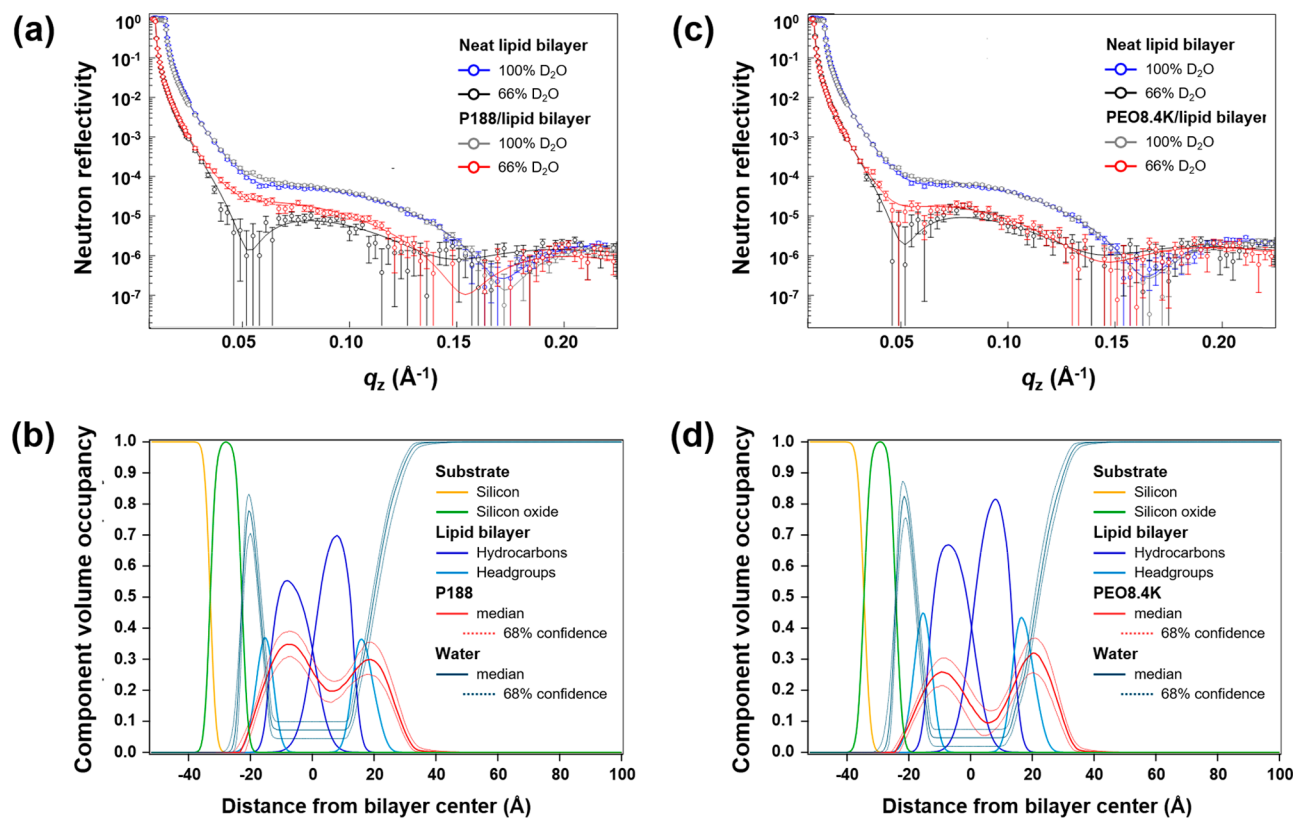


Figure 2. Neutron reflectivity (NR) data (symbols) and best model fits (solid curves) of the lipid bilayer before and after incubation with (a) P188 or (c) PEO8.4K in 100% D₂O (“D₂O-2”) and 66% D₂O. Error bars represent 68% confidence intervals for the measured reflectivity based on Poisson statistics. Component volume occupancy (CVO) profiles of (b) P188 and (d) PEO8.4K obtained from NR fitting. The median polymer and water envelopes are shown with 68% confidence intervals. A tail-deuterated POPC lipid was used for all NR measurements.

High-resolution imaging was carried out under amplitude-modulated dynamic feedback (i.e., “AC” or “tapping” mode), and the cantilever oscillation was fixed at its fundamental flexural resonance frequency. Amplitude and phase vs Z were routinely measured near the sample surface; the set point amplitude A was chosen from a range where the amplitude decreased linearly with Z . In this study, A was set to $0.83A_0$ for $2\ \mu\text{m} \times 2\ \mu\text{m}$ imaging and $0.94A_0$ for $5\ \mu\text{m} \times 5\ \mu\text{m}$ imaging, respectively, where A_0 is the oscillation amplitude of the free cantilever at resonance just off the surface (Figure S2) with calibrated values of approximately $A_0 = 1.5\ \text{nm}$ ($2\ \mu\text{m} \times 2\ \mu\text{m}$) or $6.7\ \text{nm}$ ($5\ \mu\text{m} \times 5\ \mu\text{m}$) and thereby energies of $\sim 0.5\ \text{aJ}$ ($2\ \mu\text{m} \times 2\ \mu\text{m}$) or $\sim 12.0\ \text{aJ}$ ($5\ \mu\text{m} \times 5\ \mu\text{m}$), respectively, when engaged. The Keysight software algorithm was used to set the oscillation phase of the free cantilever to 0 at resonance. By this algorithm and Keysight sign convention the phase increases to positive in the net repulsive interaction regime.³⁵ The piezo scanner Z range was reduced from the default full range ($\approx 8\ \mu\text{m}$) to $1\ \mu\text{m}$ in order to improve the digital Z binning to $0.015\ \text{nm}$. Data postprocessing and image rendering were performed using the freeware Gwyddion.³⁶

The breakthrough force of lipid bilayers with or without polymers was measured using force volume mode: an array of (quasistatic) force versus Z curves. Breakthrough force was measured at 16×16 evenly spaced locations over a $10\ \mu\text{m} \times 10\ \mu\text{m}$ bilayer area. Approach speed was $0.938\ \mu\text{m/s}$. The AFM tips were cleaned in between each force volume data set by immersing for 3 min each in isopropanol and water to remove adhered lipids or polymers on the tip surface. Deflection sensitivity (raw transducer output voltage per unit of actual tip displacement in Z) was calibrated from the contact slope of force-versus- Z scanner displacement on a rigid bare silicon substrate in buffer.³⁵ The collected data sets were analyzed using custom MATLAB code developed at the University of Minnesota Characterization Facility that will be described in detail in a forthcoming

publication. Briefly, the MATLAB code evaluates the first-order derivative of the force–distance curves after subtracting background to find the magnitude of the rupture forces. A high-pass filter is applied to the derivative to extract the abrupt changes in the derivatives that correspond to rupture forces. The values are considered as outliers if either the filtered derivative or the magnitude of the abrupt change in the force–distance curves are below certain thresholds relative to the standard deviation of the noise. The thresholds are determined by comparing the analysis results on a set of training data, i.e., selected experimental data that are manually labeled with the proper rupture positions. The thresholds are adjusted so that the analysis yields $>99\%$ correct results on all training data. The rupture forces found from force–distance curves are plotted as histograms or mapped onto 2-dimensional images. In aggregate, roughly 2300 force-vs- Z curves were compiled into histograms to analyze the statistics of stress-induced mechanical yield. Selected force- Z curves were processed into force-vs-distance units, with distance computed as the sum of Z scanner displacement and calibrated Z tip displacement (both defined as positive away from sample).

RESULTS

Critical Micelle Concentration of P188. Polymer dispersions in a buffer at $37\ ^\circ\text{C}$ were characterized using dynamic light scattering (Figure S3). The hydrodynamic radius (R_H) of P188 at $8\ \text{mmol/L}$ was $2.6\ \text{nm}$, which is close to the radius of gyration of P188 assuming a Gaussian conformation ($\approx 3\ \text{nm}$), indicating that the triblock copolymer exists as single chains at this concentration. At a concentration of $15.5\ \text{mmol/L}$ P188, peaks appeared centered around 27 and $2.8\ \text{nm}$, indicating that micelles and single chains coexist. Thus, the critical micelle concentration of P188 in a buffer solution at 37

$^{\circ}\text{C}$ is between 8 and 15.5 mmol/L. As expected, PEO exists as single polymer chains ($R_{\text{H}} = 1.9$ nm) at 16.5 mmol/L. We chose 4.5 mmol/L as the polymer concentration for NR and AFM experiments to obtain high signal-to-noise ratios while remaining below the critical micelle concentration.

Polymer Distribution within Lipid Bilayers Perpendicular to the Plane of the Membrane. The large neutron scattering contrast between hydrogen and deuterium makes NR a sensitive method to probe the distribution of polymer and lipid tail and head groups perpendicular to the plane of the bilayer. We used 1-palmitoyl-2-oleoyl-glycero-3-phosphocholine (POPC; Figure 1c), which is one of the most abundant lipids in mammalian cell membranes.³⁷ Since the neutron scattering length densities (SLDs) of P188 ($5.45 \times 10^{-7} \text{ \AA}^{-2}$) and PEO ($5.91 \times 10^{-7} \text{ \AA}^{-2}$) in the bulk state are close to that of the POPC lipid tail ($-2.88 \times 10^{-7} \text{ \AA}^{-2}$),³⁸ we employed tail-deuterated POPC (Figure 1d; $3.20 \times 10^{-6} \text{ \AA}^{-2}$) in all NR measurements to achieve greater scattering contrast with respect to the polymers. All reflectivity curves were measured using two different combinations of normal and heavy water (i.e., 100% D_2O and 66% $\text{D}_2\text{O} + 34\% \text{ H}_2\text{O}$). The resulting four NR curves of the lipid bilayer, with and without polymers and with two levels of contrast, are shown in Figure 2a,c. As the polymers are not deuterated ($\text{SLD} = 5.45 \times 10^{-7} \text{ \AA}^{-2}$), polymer addition lowers the scattering length density of the deuterated lipid tail region ($\text{SLD} = 3.20 \times 10^{-6} \text{ \AA}^{-2}$), whereas 100% D_2O water ($\text{SLD} = 6.40 \times 10^{-6} \text{ \AA}^{-2}$) incorporation raises it; for 66% D_2O , the $\text{SLD} = 4.10 \times 10^{-6} \text{ \AA}^{-2}$. These two effects counter each other to different extents with the different bulk solvents, leading to different overall changes in reflectivity. In order to effectively disentangle contributions from either effect, the simultaneous analysis of the results obtained with both solvents having different contrast was conducted. Lipids were modeled using a continuous distribution model for the lipid,³³ and polymers were modeled using a Hermite spline for the polymer²⁶ to determine the component volume occupancy (CVO) profiles that correctly describe the intermixing of molecules along the direction perpendicular to the plane of the bilayer (Figure 2b,d). Our fitting model describes the structure by real-space volume occupancy profiles, which is advantageous over conventional scattering length density profiles that are often difficult to interpret in terms of molecular structure.^{26,33} The neat lipid bilayer, cushioned by a thin water layer ($3.0 \pm 0.3 \text{ \AA}$) (Table S1), is supported by a silica substrate (ca. 1 nm thick located at the surface of a 5 mm thick silicon wafer). The total thickness of the bilayer is $\approx 50 \text{ \AA}$ with $14.6 \pm 0.4 \text{ \AA}$ of hydrophobic lipid tail, consistent with previous results.³⁸ Bilayer completeness is $99 \pm 1\%$, meaning that the lipid bilayer covers the silica substrate with less than about 1% defects or holes. After incubating a P188 solution in contact with the lipid bilayer for 2 h at $37 \text{ }^{\circ}\text{C}$ and subsequently rinsing for 45 min to remove residual polymer, the reflectivity curves showed differences from those of the neat lipid bilayer: near $q_z = 0.05 \text{ \AA}^{-1}$, where q_z is the vertical component of the momentum transfer vector, the reflectivity measured in 100% D_2O increased slightly, and the oscillation in 66% D_2O was smeared (Figure 2a). The differences are larger than the statistical error, indicating meaningful differences between the bilayers with and without P188. The NR profiles are normalized to the Fresnel reflectivity to emphasize the differences as shown in Figure S4. Reflectivities in 66% D_2O show a larger difference before and after polymer addition, which is due to the specific scattering length density values of

d_{31} -POPC hydrocarbon chains, polymer, and solvent. The distributions of polymers in the lipid bilayer were modeled by a Hermite spline without *a priori* assumptions about the shape of the curve.²⁶ In contrast to previously reported results that P188 is only weakly adsorbed on the bilayer surface, CVO profiles showed that P188 penetrates to the inner lipid headgroup (Figure 2b). Different heights and shapes of the CVO profiles of both leaflets are due to different amounts of polymer replacing lipid material. Water fills the volume not occupied by other molecular components at any position z , assuming a constant water distribution across the bilayer. Quantitatively, $32 \pm 3\%$ and $53 \pm 6\%$ of the adhered P188 resides near the lipid head and the hydrophobic tail region, respectively. The total polymer loading translates to about 9–10 polymer chains per 100 nm^2 of membrane area, obtained by dividing the volume surface density of P188 in the pure lipid bilayer ($1.27 \text{ nm}^3/\text{nm}^2$) by the molecular volume of P188 in the dry state ($13.2 \text{ nm}^3/\text{chain}$). Considering that the radius of gyration of P188 is approximately 3 nm, and assuming the triblock copolymers are uniformly distributed within the membrane (see below), the chains cannot reside in 100 nm^2 without overlapping each other. This implies that the polymer chains are interwoven with lipid molecules with significant overlap. The thickness of the lipid tail region decreased by $2.0 \pm 0.4 \text{ \AA}$ upon P188 adsorption. Bilayer completeness decreased to $93 \pm 3\%$, indicating that some solvent molecules entered the hydrophobic region. This might result from either the insertion of P188 chains bearing water molecules or the removal of lipid molecules due to the high local concentration of P188. The bilayer completeness of 93% is still remarkable considering that a high concentration (4.5 mmol/L) of P188 was used. The volume fraction of P188 outside the lipid bilayer is $13 \pm 3\%$ of the total adhered amount (Table S1). Best-fit nSLD profiles for all measurements are presented in Figure S5. We excluded the possibility of multilayer stacking upon polymer addition because multilayers would lead to Bragg peaks in the reflectivity data that are easily identified and could not be modeled with a single bilayer model. In addition, the AFM measurements produced a peak force during breakthrough experiments (see below) at a single distance (ca. 4 nm) above the substrate at all lateral positions when the AFM tip approached the lipid bilayer, consistent with a single lipid bilayer.

Note that a significant amount of P188 remained in the lipid bilayer after rinsing the surface, as confirmed by sequential solvent exchange. After the initial polymer incubation and rinsing, NR measurements were performed with 100% D_2O buffer first (“ D_2O -1”), followed by 66% D_2O , and back to 100% D_2O (“ D_2O -2”). The 66% D_2O data were paired with either D_2O -1 (Figure S6a,b) or D_2O -2 (Figure 2a,b) for simultaneous fitting. Although there is a slight decrease in volume occupancy of P188, the polymer mostly (>90%) remains in the lipid bilayer even after multiple rinses. Also, the CVO profile (Figure S6b) and fit values (Table S2) did not change significantly. This result is consistent with our previous study using surface plasmon resonance spectroscopy, which showed that the adhered polymers were not removed from the lipid bilayer after rinsing.²³

Unexpectedly, PEO8.4K also penetrated to the inner lipid headgroup with a distribution profile similar to that of P188 when incubated using the same procedure (Figure 2c,d). The NR curves obtained after contacting 4.5 mmol/L PEO8.4K with the lipid bilayer show the same trends as with P188: upon

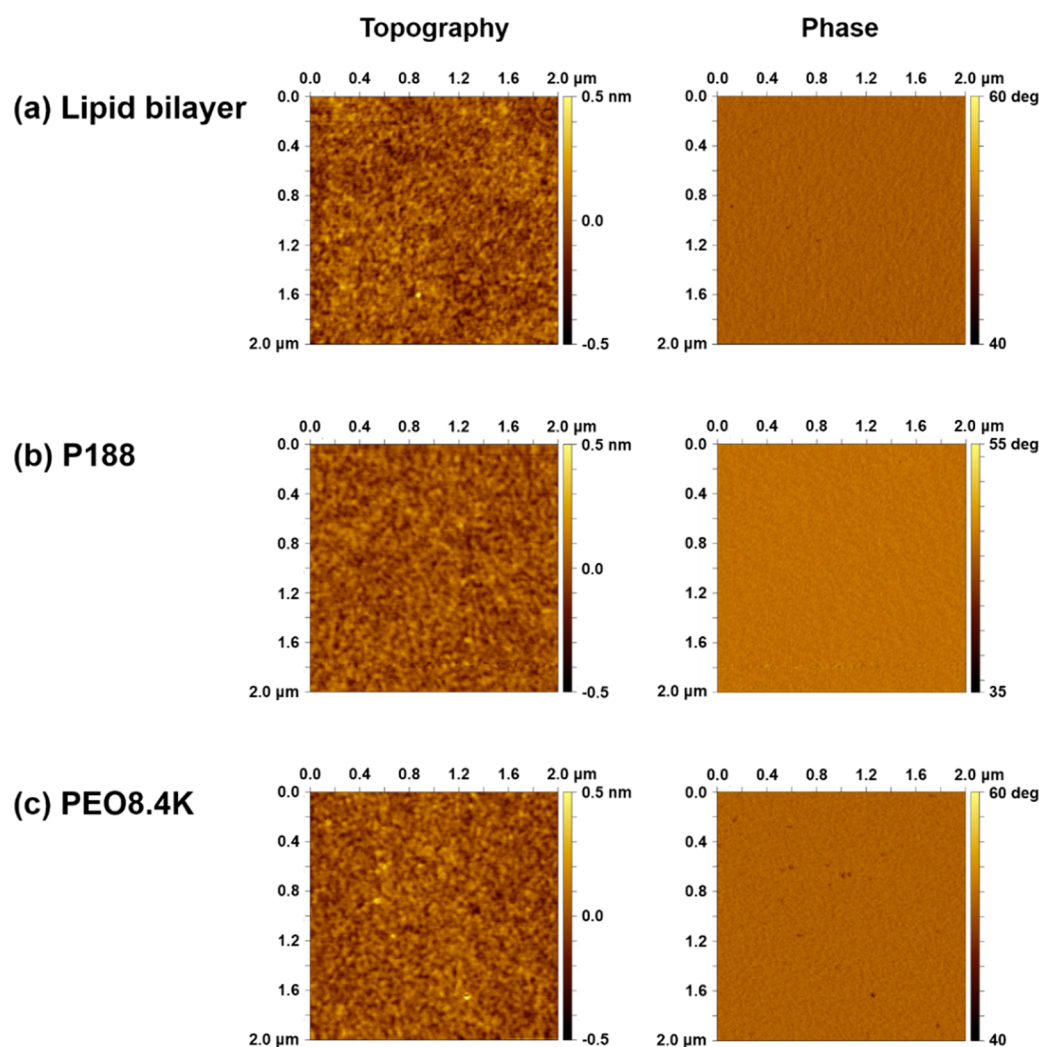


Figure 3. Topography and phase images ($2 \mu\text{m} \times 2 \mu\text{m}$, 512×512 pixels) of lipid bilayers before and after incubation with polymers measured using atomic force microscopy: (a) neat lipid bilayer, (b) P188-incubated bilayer, and (c) PEO8.4K-incubated bilayer.

polymer incubation and rinsing, NR curves of PEO8.4K/lipid bilayer deviated from that of neat lipid bilayer in both 100% and 66% D_2O , particularly near $q_z = 0.05 \text{ \AA}^{-1}$ (Figure 2c). The difference between the neat lipid bilayer with and without PEO8.4K is statistically significant, although changes in reflectivity are larger for P188 due to a larger amount of polymer addition. The NR profiles are normalized to the Fresnel reflectivity to emphasize the differences in Figure S4. The resulting CVO profile (Figure 2d) of the PEO8.4K-incubated lipid bilayer has similar features to that of the P188-incubated counterpart. The fitted parameters (Table S3) are also close to the values obtained for the P188-incubated lipid bilayer (Table S1). A significant amount of PEO8.4K remained inside the lipid bilayer after multiple rinses (Figure S6c,d and Table S4).

Surface Morphology and Breakthrough Forces of Lipid Bilayers with or without Polymers. NR probes vertical profiles while averaging the in-plane structural features over the entire illumination area of ca. $2.5 \times 5 \text{ cm}^2$ that is probed by neutron wave packets (each having coherence area of ca. $10 \times 400 \mu\text{m}^2$).³⁹ Based on NR alone, it would not be possible to ascertain whether the adsorbed polymers form laterally phase-separated domains in the polymer/lipid films. We used AFM as a complementary tool to probe the surface

morphology of lipid bilayers upon polymer incubation. The surface morphology was obtained using AC mode with set point amplitude ratio $A/A_0 = 0.83$ (for $2 \mu\text{m} \times 2 \mu\text{m}$ imaging) where A is the set point cantilever oscillation amplitude when feedback-engaged with the surface, and A_0 is the amplitude of the free cantilever. Both phase images and phase-Z curves (where Z is the scanner displacement) indicated operation in the net repulsive regime (Figure S2).³⁵ Under this measurement condition, the cantilever tip interacts with the surface minimally during raster scanning ($<1 \mu\text{s}$ per oscillation cycle) to avoid perturbing the surface morphology with shear forces. The high set point amplitude ratio further minimizes morphological perturbation via normal forces (variable amplitude reduction vs Z). As expected from the NR result (i.e., 99% bilayer completeness), the surface of the neat lipid bilayer was extremely smooth with height variation within $\pm 5 \text{ \AA}$ over $4 \mu\text{m}^2$ regions (Figure 3a), which mirrors the roughness of the bare silicon wafer; for example, the root-mean-square (RMS) roughness (standard deviation of height) of both surfaces was 84 pm.

4.5 mmol/L P188 and PEO8.4K were exposed to the bilayer using the same protocol as for the NR sample preparation: incubation at $37 \text{ }^\circ\text{C}$ for 2 h followed by rinsing off residual polymers before the samples were subjected to the AFM

imaging. We prepared at least 10 replicas of each sample (i.e., lipid bilayers with or without polymer incubation) and probed 2–3 regions of each surface. None of the topography images on either P188- or PEO-incubated surfaces (Figure 3b,c) showed any holes or defects greater than the estimated resolution calculated using the nominal tip radius³⁵ of ca. 8 nm; this is also consistent with the NR analysis where the bilayer completeness was fitted to be $\approx 90\%$ for both systems. The height variations were within ± 5 Å, and the RMS roughness values were 70 and 74 pm for P188- and PEO-incubated lipid bilayers, respectively. In addition, the phase images did not exhibit any noteworthy contrast (clarified below), indicating that the polymer-incubated surfaces are essentially single-phase. As phase changes with surface mechanical properties (i.e., existence of different materials on the surface), the featureless images imply the absence of surface heterogeneity. The topography and phase images of a large-area scan ($5 \mu\text{m} \times 5 \mu\text{m}$) also did not have any specific features greater than the AFM resolution, confirming that all surfaces are homogeneous (Figure S7). Thus, we confirmed that P188 and PEO8.4K do not form macroscopic phase-separated domains larger than the lateral resolution of the AFM measurements (≤ 10 nm). Macroscopic phase separation of the polymers would produce much larger domains, which would not be constrained to the ca. 4 nm film thickness identified in Figure 2. Also, the dynamic light scattering (DLS) measurements show that P188 micelles (that form at 15.5 mmol/L) have a diameter of about 55 nm, which would be plainly evident in the AFM scans if present. Note that the small features on the surfaces of neat and PEO-incubated lipid bilayers (appearing as sub 100 nm dark regions in the phase images in Figure 3a,c) are not phase-separated domains, as they also appear on polymer-free bilayers (and only sporadically among the many samples examined of all types, thus representing infrequent contamination).

Besides the AC mode for probing surface morphology, we used force-volume mode to measure the rupture force of the lipid bilayer with and without polymers. In this method, over an array of locations (here 16×16 evenly distributed over $10 \mu\text{m} \times 10 \mu\text{m}$), the AFM tip first approaches and presses the lipid bilayer until penetrating to the surface and reaching the silicon wafer, a stress-induced mechanical yield event under measurable quasistatic force (Scheme 1). The force required for the tip to produce mechanical yield is here termed the “breakthrough force”. To check for tip-state effects (contamination by polymer or lipid molecules), the breakthrough force on the neat lipid bilayer was measured both *before and after* measuring that on the polymer-incubated surfaces and considered reproducible (tip unmodified) if the two results were consistent. In 4 out of 5 regions explored, the distribution of breakthrough force did not change significantly upon P188 or PEO8.4K incubation (Figure 4a,b). The spatial distributions of the breakthrough forces were essentially homogeneous (Figure S8), which also supports our conclusion that there are no defects or phase-separated domains. Representative force–distance curves when the tip approaches the lipid bilayer are shown in Figure 4c, where the zero distance is set as the underlying rigid silicon oxide surface. In the case of the neat lipid bilayer, the AFM tip started to interact with the bilayer surface at around 6 nm and ruptured the bilayer at around 4 nm with 5.5 nN breakthrough force. The force–distance curves for polymer-incubated surfaces were essentially the same, which is reasonable because the NR results show that

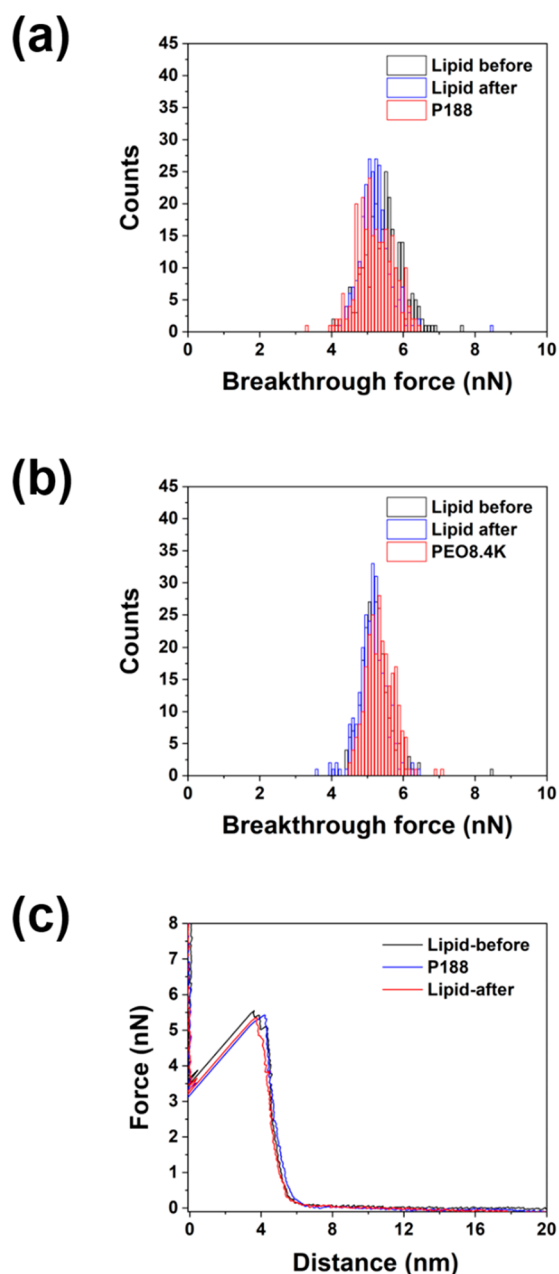


Figure 4. Breakthrough force measurement with AFM. The force obtained from the neat lipid bilayer measured before and after measuring that for a polymer-incubated bilayer using the same tip is denoted as “Lipid before” or “Lipid after”, respectively. Histograms of breakthrough force obtained for (a) neat vs P188-incubated bilayer and (b) neat vs PEO8.4K-incubated bilayer. (c) Representative force–distance curves when the tip approaches and breaks through the bilayer surface.

only a small fraction of the adsorbed polymers was outside the lipid bilayer. Remarkably, the presence of ca. 30% by volume of P188 or PEO did not change the force required to disrupt the bilayer membrane.

DISCUSSION

We found that most P188 and PEO8.4K chains reside within the planar lipid bilayer, down to the inner lipid head region. No phase-separated domains, defects, or holes were observed on the surfaces of polymer-incubated lipid bilayers, implying

that both polymers mingle with lipid molecules homogeneously (Figure 5). Remarkably, the planar lipid bilayer was

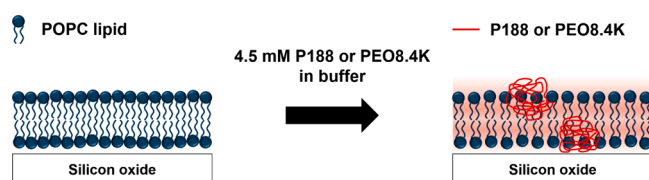


Figure 5. Proposed distribution of polymers in the lipid bilayer. Since the neutron scattering length density of PPO and PEO are nearly indistinguishable, polymers coils are drawn using a single color.

able to hold $\approx 30\%$ by volume of polymer without losing structural integrity. Also, significant amounts of both polymers remained inside the bilayer after several rinse steps over the total NR measurement time of ≈ 18 h. Collectively these results indicate that P188 and PEO8.4K can penetrate intact lipid bilayers. This finding is seemingly contradictory to a previous study on a lipid monolayer at an air/water interface, which proposed that P188 inserted only into damaged membranes and was squeezed out when membrane integrity was restored.⁴⁰ X-ray reflectivity and grazing incidence X-ray scattering results suggested that the P188 phase separated from the lipid monolayer at the air/water interface.^{41,42} However, a monolayer is qualitatively different than a bilayer and does not directly mimic a cell plasma membrane because it does not have features found in bilayers such as lipid flip-flop and interleaflet coupling.⁴³ In addition, some *in vitro* and *in vivo* studies reported that P188 could protect cell membranes only when the polymer was added to the system before injuring or stressing the membrane,^{13,17} suggesting that P188 interacts with an intact lipid bilayer, not only with a damaged membrane.

Combining the current results with previous studies using molecular dynamics (MD) simulations, we propose the following binding process of P188/PEO8.4K to a lipid bilayer. In aqueous solution, P188 adopts random coil configurations in which the PEO blocks wrap preferentially around the outside of the molecule. When P188 approaches the lipid bilayer, PEO is the first part of the molecule to interact with the lipid head groups. Based on our finding that PEO8.4K also inserts in the lipid bilayer, PEO is the key chemical moiety that drives initial P188 binding to the lipid bilayer. A coarse-grained MD simulation of P188 interacting with a 1,2-dilauroyl-*sn*-glycero-3-phosphocholine (DLPC) lipid bilayer showed that PEO chains interact with lipid head groups, and PPO is partially inserted into the hydrophobic region within 800 ns of simulation time.⁴⁴ Another 100 ns atomistic simulation using a POPC lipid bilayer showed a similar result.⁴⁵ In this case, the bilayer was stretched to enable the P188 insertion within the limited amount of simulation time. The MD simulations are usually limited to hundreds of nanoseconds because of computational expense, so the results represent the early stages of the polymer–lipid bilayer interactions. Our NR results, obtained after incubating for 2 h, represent the steady-state distribution of the P188, which can be achieved when the partially inserted polymers diffuse into the inner leaflet of the lipid bilayer. There are few simulation studies on PEO–lipid interactions. One 700 ns simulation with 8000 g/mol PEO and 1,2-dioleoyl-*sn*-glycero-3-phosphocholine (DOPC) lipid bilayer showed that the PEO made contact but was not inserted

into the lipid bilayer, within the simulation time.⁴⁶ Our NR study indicates that the PEO8.4K also inserts into the lipid bilayer when incubated for sufficient time.

The deep penetration of P188 and its homogeneous interaction with lipid molecules support the hypothesis that inserted polymer chains can deter lateral diffusion of the lipid molecules. Reduced lateral diffusion (reduced by $\sim 10\%$ compared to neat bilayer at 100 μM P188 concentration) was reported in previous studies that measured lipid diffusion after polymer binding using fluorescent recovery after photobleaching.⁴⁷

Why do both P188 and PEO8.4K penetrate into the inner leaflet? Although usually considered to be hydrophilic, PEO is an amphiphilic chemical moiety⁴⁸ in which hydrophobicity is conferred from CH_2 groups, and hydrophilicity comes from oxygen atoms associated with the ether groups. Each ether moiety can hydrogen bond with 1–6 water molecules.⁴⁹ PEO homopolymers and Poloxamers (including P188) become more hydrophobic with increasing salt concentration in aqueous solutions.^{50–53} This can be attributed to the dehydration of polymer molecules resulting from the change of hydrogen bonding between water and the polymers at elevated salt concentration. As charged molecules are likely to attract more water molecules than nonionic Poloxamers or PEO, the polymers will become less soluble in water. We hypothesize that the dehydration of polymers occurs in a similar manner when the polymers interact with charged headgroups of the lipid, which would render the polymers more hydrophobic and enable diffusion to the inner lipid head groups and lipid tails.

The release of water molecules from the polymers during dehydration is expected to increase the entropy of binding. A previous study measured the molar enthalpy of binding ($\Delta H_{\text{binding}}$) of Poloxamer 338 (P338) to 1,2-dimyristoyl-*sn*-glycero-3-phosphocholine (DMPC) liposomes, where P338 has double the molecular weight of P188 with the same weight percent of PEO (80% by mass).^{54,55} The measured $\Delta H_{\text{binding}}$ was +53.6 kJ/mol, indicating that the binding of P338 to the lipid bilayer is enthalpically unfavorable.^{54,55} Thus, a potential entropic increase by the release of water molecules from polymers might be a key driving force for the binding event. Also, our previous study using SPR found that a 2000 g/mol PEO homopolymer does not bind to lipid bilayers, whereas an 8600 g/mol PEO homopolymer does.²³ This can be rationalized based on a reduced loss of combinatorial entropy in solution upon adsorption of higher-molecular-weight polymer. Indeed, there seems to be a PEO molecular weight dependence on cell membrane protection. A previous study reported that high-molecular-weight PEO homopolymer (molar mass range 15 000–20 000 g/mol) protects cardiac myocytes from hypoxia-reoxygenation injuries, potentially through membrane stabilization.⁵⁶

As noted earlier, PEO8.4K does not protect cell membranes under physiological conditions despite the similar binding behavior to model lipid bilayer as P188, under the conditions employed in this study. As revealed in our previous report, the average surface coverage of P188 on a POPC bilayer decreased around 5-fold as the polymer concentration was reduced from 4.5 to 150 $\mu\text{mol/L}$.²³ Moreover, we have shown that the surface coverage of P188 on 50 to 100 nm diameter POPC bilayer liposomes falls to an area coverage of 42 nm^2 per adsorbed block copolymer, when the concentration in aqueous solution reaches 120 $\mu\text{mol/L}$.²² In these limits (much closer to

the concentrations employed with living organisms), the adsorbed chains do not overlap on average, which may amplify the role of the hydrophobic PPO block in positioning the block copolymer within the hydrocarbon portion of the membrane. Another possible reason is that cell membrane constituents other than the lipid molecules (e.g., cholesterol) might interfere with PEO8.4K binding to the bilayer. A recent study by our group using POPC liposomes revealed a dramatic reduction in the binding of various Ploxadimers as the concentration of cholesterol was increased beyond 20 mol % relative to lipid.⁵⁷ These two effects may operate in concert at therapeutic doses in living tissue.

This study provides important clues as to how P188 and PEO8.4K interact with and penetrate lipid bilayers. The ability to uniformly load 30% by volume of these polymers into the bilayer without membrane disruption, and retention of mechanical resistance to AFM tip penetration, suggests that favorable interactions among the lipid, PEO, and PPO chains play an integral role in cell membrane protection. Once the polymer chains adhere to and diffuse into the lipid bilayer, the polymer chains would be able to tether lipid molecules and prevent the membrane from being torn apart when subjected to external stress. Also, when a membrane is disrupted, lipid molecules instantly rearrange to minimize exposure of the hydrophobic tails to aqueous solution, forming stable pores that are a source of increased permeability across the membrane. Pore formation may be prevented by the presence of the amphiphilic block copolymer chains, which can shield lipid tail exposure to water when a stress is applied to the membrane.

CONCLUSIONS

We studied the distribution of P188 and PEO8.4K in supported POPC lipid bilayers using neutron reflectivity and atomic force microscopy after incubation with 4.5 mmol/L buffered aqueous polymer solutions, followed by rinsing with the aqueous medium. Both polymers were confirmed by dynamic light scattering to exist in solution as single chains at 4.5 mmol/L. Analysis of the NR results revealed that both P188 and PEO8.4K penetrate into the lipid bilayer, centered close to the polar head groups but also reaching into the inner hydrophobic lipid core, in contrast to earlier reports indicating that P188, at lower concentrations in water, only partially penetrates the lipid membranes or adheres only to the membrane surface.^{19,20} Both polymer chains remained in the lipid bilayer after multiple rinses with buffer solution, indicating that the polymers bind nearly irreversibly (i.e., on the time scale of the experiments) to the membrane, consistent with our previous study that investigated polymer binding kinetics using surface plasmon resonance spectroscopy.²³

Lipid bilayers were examined using AFM before and after polymer incubation, confirming the absence of defects or phase-separated domains, demonstrating that both P188 and PEO8.4K chains mingle homogeneously with the lipid molecules in the bilayer at length scales comparable to the polymer coil dimension. Remarkably, the breakthrough force of the lipid membranes measured by AFM did not change upon polymer incubation, notwithstanding 30% by volume loading demonstrated by NR. These findings provide fresh insight into the nature of the interactions that govern adsorption of P188 and PEO into lipid bilayer membranes and contribute to the quest to understand how these amphiphilic compounds protect cell membranes.

ASSOCIATED CONTENT

Supporting Information

The Supporting Information is available free of charge at <https://pubs.acs.org/doi/10.1021/acs.langmuir.9b03208>.

Dynamic light scattering data; ¹NMR and MALDI data; AFM results; and neutron reflectivity data, modeling parameters, and fits (PDF)

AUTHOR INFORMATION

Corresponding Authors

Greg Haugstad – Characterization Facility, University of Minnesota, Minneapolis, Minnesota 55455, United States; Email: haugs001@umn.edu

Frank S. Bates – Department of Chemical Engineering and Materials Science, University of Minnesota, Minneapolis, Minnesota 55455, United States; orcid.org/0000-0003-3977-1278; Email: bates001@umn.edu

Authors

Mihee Kim – Department of Chemical Engineering and Materials Science, University of Minnesota, Minneapolis, Minnesota 55455, United States

Frank Heinrich – Department of Physics, Carnegie Mellon University, Pittsburgh, Pennsylvania 15213, United States; National Institute of Standards and Technology Center for Neutron Research, Gaithersburg, Maryland 20899, United States

Guichuan Yu – Informatics Institute, University of Minnesota, Minneapolis, Minnesota 55455, United States

Guangcui Yuan – National Institute of Standards and Technology Center for Neutron Research, Gaithersburg, Maryland 20899, United States; Department of Physics, Georgetown University, Washington, D.C. 20057, United States

Sushil K. Satija – National Institute of Standards and Technology Center for Neutron Research, Gaithersburg, Maryland 20899, United States

Wenjia Zhang – Department of Chemical Engineering and Materials Science, University of Minnesota, Minneapolis, Minnesota 55455, United States; orcid.org/0000-0002-8930-2480

Hannah S. Seo – Department of Chemical Engineering and Materials Science, University of Minnesota, Minneapolis, Minnesota 55455, United States

Joseph M. Metzger – Department of Integrative Biology and Physiology, University of Minnesota Medical School, Minneapolis, Minnesota 55455, United States; orcid.org/0000-0002-3882-4326

Samira M. Azarin – Department of Chemical Engineering and Materials Science, University of Minnesota, Minneapolis, Minnesota 55455, United States; orcid.org/0000-0003-0395-4988

Timothy P. Lodge – Department of Chemical Engineering and Materials Science and Department of Chemistry, University of Minnesota, Minneapolis, Minnesota 55455, United States; orcid.org/0000-0001-5916-8834

Benjamin J. Hackel – Department of Chemical Engineering and Materials Science, University of Minnesota, Minneapolis, Minnesota 55455, United States; orcid.org/0000-0003-3561-9463

Complete contact information is available at: <https://pubs.acs.org/doi/10.1021/acs.langmuir.9b03208>

Notes

The authors declare the following competing financial interest(s): J.M.M. is on the scientific advisory board of and holds zero value equity shares in Phrixus Pharmaceuticals Inc., a company developing novel therapeutics for heart failure and DMD, and this is actively managed by the UMN Office of Institutional Compliance.

ACKNOWLEDGMENTS

This work was supported by a grant from the National Institutes of Health (R01 HL122323 and R01 AR071349). The AFM experiments were conducted at the Characterization Facility, University of Minnesota, which receives partial support from the NSF through the MRSEC program (DMR-1420013). We acknowledge the support of the National Institute of Standards and Technology (NIST), U.S. Department of Commerce, in providing the neutron research facilities used in this work. Certain commercial equipment, instruments, or materials are identified in this paper to foster understanding. Such identification does not imply recommendation or endorsement by the NIST, nor does it imply that the materials or equipment identified are necessarily the best available for the purpose. H.S.S. is supported by a Graduate Research Fellowship from the National Science Foundation under Grant 00039202.

REFERENCES

- (1) McNeil, P. L.; Steinhardt, R. A. Plasma Membrane Disruption: Repair, Prevention, Adaptation. *Annu. Rev. Cell Dev. Biol.* **2003**, *19*, 697–731.
- (2) Lee, R. C.; River, L. P.; Pan, F. S.; Ji, L.; Wollmann, R. L. Surfactant-Induced Sealing of Electroporabilized Skeletal Muscle Membranes in Vivo. *Proc. Natl. Acad. Sci. U. S. A.* **1992**, *89*, 4524–4528.
- (3) Kim, M.; Haman, K. J.; Houang, E. M.; Zhang, W.; Yannopoulos, D.; Metzger, J. M.; Bates, F. S.; Hackel, B. J. PEO–PPO Diblock Copolymers Protect Myoblasts from Hypo-Osmotic Stress In Vitro Dependent on Copolymer Size, Composition, and Architecture. *Biomacromolecules* **2017**, *18*, 2090–2101.
- (4) Wong, S. W.; Yao, Y.; Hong, Y.; Ma, Z.; Kok, S. H. L.; Sun, S.; Cho, M.; Lee, K. K. H.; Mak, A. F. T. Preventive Effects of Poloxamer 188 on Muscle Cell Damage Mechanics Under Oxidative Stress. *Ann. Biomed. Eng.* **2017**, *45*, 1083–1092.
- (5) Chang, D.; Fox, R.; Hicks, E.; Ferguson, R.; Chang, K.; Osborne, D.; Hu, W.; Velev, O. D. Investigation of Interfacial Properties of Pure and Mixed Poloxamers for Surfactant-Mediated Shear Protection of Mammalian Cells. *Colloids Surf., B* **2017**, *156*, 358–365.
- (6) Collins, J. M.; Despa, F.; Lee, R. C. Structural and Functional Recovery of Electroporabilized Skeletal Muscle In-Vivo after Treatment with Surfactant Poloxamer 188. *Biochim. Biophys. Acta, Biomembr.* **2007**, *1768*, 1238–1246.
- (7) Merchant, F. a; Holmes, W. H.; Capelli-Schellpfeffer, M.; Lee, R. C.; Toner, M. Poloxamer 188 Enhances Functional Recovery of Lethally Heat-Shocked Fibroblasts. *J. Surg. Res.* **1998**, *74*, 131–140.
- (8) Wang, T.; Chen, X.; Wang, Z.; Zhang, M.; Meng, H.; Gao, Y.; Luo, B.; Tao, L.; Chen, Y. Poloxamer-188 Can Attenuate Blood–Brain Barrier Damage to Exert Neuroprotective Effect in Mice Intracerebral Hemorrhage Model. *J. Mol. Neurosci.* **2015**, *55*, 240–250.
- (9) Platakis, M.; Lee, Y. D.; Rasmussen, D. L.; Hubmayr, R. D. Poloxamer 188 Facilitates the Repair of Alveolus Resident Cells in Ventilator-Injured Lungs. *Am. J. Respir. Crit. Care Med.* **2011**, *184*, 939.
- (10) Luo, C.-L.; Chen, X.-P.; Li, L.-L.; Li, Q.-Q.; Li, B.-X.; Xue, A.-M.; Xu, H.-F.; Dai, D.-K.; Shen, Y.-W.; Tao, L.-Y.; Zhao, Z.-Q. Poloxamer 188 Attenuates In Vitro Traumatic Brain Injury-Induced

Mitochondrial and Lysosomal Membrane Permeabilization Damage in Cultured Primary Neurons. *J. Neurotrauma* **2013**, *30*, 597–607.

- (11) Yasuda, S.; Townsend, D.; Michele, D. E.; Favre, E. G.; Day, S. M.; Metzger, J. M. Dystrophic Heart Failure Blocked by Membrane Sealant Poloxamer. *Nature* **2005**, *436*, 1025–1029.

- (12) Markham, B. E.; Kernodle, S.; Nemzek, J.; Wilkinson, J. E.; Sigler, R. Chronic Dosing with Membrane Sealant Poloxamer 188 NF Improves Respiratory Dysfunction in Dystrophic Mdx and Mdx/Utrophin^{-/-} Mice. *PLoS One* **2015**, *10*, e0134832.

- (13) Martindale, J. J.; Metzger, J. M. Uncoupling of Increased Cellular Oxidative Stress and Myocardial Ischemia Reperfusion Injury by Directed Sarcolemma Stabilization. *J. Mol. Cell. Cardiol.* **2014**, *67*, 26–37.

- (14) Houang, E. M.; Haman, K. J.; Filaretto, A.; Perlingeiro, R. C.; Bates, F. S.; Lowe, D. A.; Metzger, J. M. Membrane-Stabilizing Copolymers Confer Marked Protection to Dystrophic Skeletal Muscle in Vivo. *Mol. Ther.–Methods Clin. Dev.* **2015**, *2*, 15042.

- (15) Houang, E. M.; Sham, Y. Y.; Bates, F. S.; Metzger, J. M. Muscle Membrane Integrity in Duchenne Muscular Dystrophy. *Skeletal Muscle* **2018**, *8*, 1–19.

- (16) Bartos, J. A.; Matsuura, T. R.; Sarraf, M.; Youngquist, S. T.; McKnite, S. H.; Rees, J. N.; Sloper, D. T.; Bates, F. S.; Segal, N.; Debaty, G.; Lurie, K. G.; Neumar, R. W.; Metzger, J. M.; Riess, M. L.; Yannopoulos, D. Bundled Postconditioning Therapies Improve Hemodynamics and Neurologic Recovery after 17 min of Untreated Cardiac Arrest. *Resuscitation* **2015**, *87*, 7–13.

- (17) Bartos, J. A.; Matsuura, T. R.; Tsangaris, A.; Olson, M.; McKnite, S. H.; Rees, J. N.; Haman, K.; Shekar, K. C.; Riess, M. L.; Bates, F. S.; Metzger, J. M.; Yannopoulos, D. Intracoronary Poloxamer 188 Prevents Reperfusion Injury in a Porcine Model of ST-Segment Elevation Myocardial Infarction. *JACC Basic to Transl. Sci.* **2016**, *1*, 224–234.

- (18) Houang, E. M.; Bartos, J.; Hackel, B. J.; Lodge, T. P.; Yannopoulos, D.; Bates, F. S.; Metzger, J. M. Cardiac Muscle Membrane Stabilization in Myocardial Reperfusion Injury. *JACC Basic to Transl. Sci.* **2019**, *4*, 275–287.

- (19) Lee, B.; Firestone, M. A. Electron Density Mapping of Triblock Copolymers Associated with Model Biomembranes: Insights into Conformational States and Effect on Bilayer Structure. *Biomacromolecules* **2008**, *9*, 1541–1550.

- (20) Firestone, M. A.; Wolf, A. C.; Seifert, S. Small-Angle X-Ray Scattering Study of the Interaction of Poly(Ethylene Oxide)-b-Poly(Propylene Oxide)-b-Poly(Ethylene Oxide) Triblock Copolymers with Lipid Bilayers. *Biomacromolecules* **2003**, *4*, 1539–1549.

- (21) Cheng, C.; Wang, J.; Kausik, R.; Lee, K. Y. C.; Han, S. Nature of Interactions between PEO-PPO-PEO Triblock Copolymers and Lipid Membranes: (II) Role of Hydration Dynamics Revealed by Dynamic Nuclear Polarization. *Biomacromolecules* **2012**, *13*, 2624–2633.

- (22) Zhang, W.; Haman, K. J.; Metzger, J. M.; Hackel, B. J.; Bates, F. S.; Lodge, T. P. Quantifying Binding of Ethylene Oxide-Propylene Oxide Block Copolymers with Lipid Bilayers. *Langmuir* **2017**, *33*, 12624–12634.

- (23) Kim, M.; Vala, M.; Ertsgaard, C. T.; Oh, S.; Lodge, T. P.; Bates, F. S.; Hackel, B. J. Surface Plasmon Resonance Study of the Binding of PEO–PPO–PEO Triblock Copolymer and PEO Homopolymer to Supported Lipid Bilayers. *Langmuir* **2018**, *34*, 6703–6712.

- (24) Zhao, Z.; Ji, X.; Dimova, R.; Lipowsky, R.; Liu, Y. Viscoelasticity of Poly(Ethylene Glycol) Solutions on Supported Lipid Bilayers via Quartz Crystal Microbalance with Dissipation. *Macromolecules* **2015**, *48*, 1824–1831.

- (25) Kakimoto, Y.; Tachihara, Y.; Okamoto, Y.; Miyazawa, K.; Fukuma, T.; Tero, R. Morphology and Physical Properties of Hydrophilic-Polymer-Modified Lipids in Supported Lipid Bilayers. *Langmuir* **2018**, *34*, 7201.

- (26) Heinrich, F.; Lösche, M. Zooming in on Disordered Systems: Neutron Reflection Studies of Proteins Associated with Fluid Membranes. *Biochim. Biophys. Acta, Biomembr.* **2014**, *1838*, 2341–2349.

- (27) Picas, L.; Milhiet, P.; Hernández-borrell, J. Atomic Force Microscopy: A Versatile Tool to Probe the Physical and Chemical Properties of Supported Membranes at the Nanoscale. *Chem. Phys. Lipids* **2012**, *165*, 845–860.
- (28) Ho, R. J. Y.; Schmetz, M.; Deamer, D. W. Nonenzymatic Hydrolysis of Phosphatidylcholine Prepared as Liposomes and Mixed Micelles. *Lipids* **1987**, *22*, 156–158.
- (29) Boggara, M. B.; Faraone, A.; Krishnamoorti, R. Effect of pH and Ibuprofen on the Phospholipid Bilayer Bending Modulus. *J. Phys. Chem. B* **2010**, *114*, 8061–8066.
- (30) Naumowicz, M.; Figaszewski, Z. A. The Effect of pH on the Electrical Capacitance of Phosphatidylcholine–Phosphatidylserine System in Bilayer Lipid Membrane. *J. Membr. Biol.* **2014**, *247*, 361–369.
- (31) Nicolai, T.; Brown, W.; Johnsen, R. M.; Stepanek, P. Dynamic Behavior of θ Solutions of Polystyrene Investigated by Dynamic Light Scattering. *Macromolecules* **1990**, *23*, 1165–1174.
- (32) Parratt, L. G. Surface Studies of Solids by Total Reflection of X-Rays. *Phys. Rev.* **1954**, *95*, 359–369.
- (33) Kirby, B.J.; Kienzle, P.A.; Maranville, B.B.; Berk, N.F.; Krycka, J.; Heinrich, F.; Majkrzak, C.F. Phase-sensitive specular neutron reflectometry for imaging the nanometer scale composition depth profile of thin-film materials. *Curr. Opin. Colloid Interface Sci.* **2012**, *17*, 44–53.
- (34) Heinrich, F.; Ng, T.; Vanderah, D. J.; Shekhar, P.; Mihailescu, M.; Nanda, H.; Lösche, M. A New Lipid Anchor for Sparsely Tethered Bilayer Lipid Membranes. *Langmuir* **2009**, *25*, 4219–4229.
- (35) Haugstad, G. D. *Atomic Force Microscopy: Understanding Basic Modes and Advanced Applications*; John Wiley & Sons, Inc.: Hoboken, NJ, 2012.
- (36) Nečas, D.; Klapetek, P. Gwyddion: An Open-Source Software for SPM Data Analysis. *Open Phys.* **2012**, *10*, s11534.
- (37) Harayama, T.; Riezman, H. Understanding the Diversity of Membrane Lipid Composition. *Nat. Rev. Mol. Cell Biol.* **2018**, *19*, 281–296.
- (38) Benedetto, A.; Heinrich, F.; Gonzalez, M. A.; Fragneto, G.; Watkins, E.; Ballone, P. Structure and Stability of Phospholipid Bilayers Hydrated by a Room-Temperature Ionic Liquid/Water Solution: A Neutron Reflectometry Study. *J. Phys. Chem. B* **2014**, *118*, 12192–12206.
- (39) Majkrzak, C. F.; Metting, C.; Maranville, B. B.; Dura, J. A.; Satija, S.; Udovic, T.; Berk, N. F. Determination of the Effective Transverse Coherence of the Neutron Wave Packet as Employed in Reflectivity Investigations of Condensed-Matter Structures. *Phys. Rev. A: At., Mol., Opt. Phys.* **2014**, *89*, No. 033851.
- (40) Maskarinec, S. A.; Lee, R. C.; Lee, K. Y. C. Direct Observation of Poloxamer 188 Insertion into Lipid Monolayers. *Biophys. J.* **2002**, *82*, 1453–1459.
- (41) Wu, G.; Majewski, J.; Ege, C.; Kjaer, K.; Weygand, M. J.; Lee, K. Y. C. Lipid Corralling and Poloxamer Squeeze-Out in Membranes. *Phys. Rev. Lett.* **2004**, *93*, 2–5.
- (42) Wu, G.; Majewski, J.; Ege, C.; Kjaer, K.; Weygand, J.; Lee, K. Y. C. Interaction between Lipid Monolayers and Poloxamer 188: An X-Ray Reflectivity and Diffraction Study. *Biophys. J.* **2005**, *89*, 3159–3173.
- (43) Fujimoto, T.; Parmryd, I. Interleaflet Coupling, Pinning, and Leaflet Asymmetry—Major Players in Plasma Membrane Nanodomain Formation. *Front. Cell Dev. Biol.* **2017**, 155.
- (44) Goliaei, A.; Lau, E. Y.; Adhikari, U.; Schwegler, E.; Berkowitz, M. L. Behavior of P85 and P188 Poloxamer Molecules: Computer Simulations Using United-Atom Force-Field. *J. Phys. Chem. B* **2016**, *120*, 8631–8641.
- (45) Houang, E. M.; Bates, F. S.; Sham, Y. Y.; Metzger, J. M. All-Atom Molecular Dynamics-Based Analysis of Membrane-Stabilizing Copolymer Interactions with Lipid Bilayers Probed under Constant Surface Tensions. *J. Phys. Chem. B* **2017**, *121*, 10657–10664.
- (46) Liu, Y.; Agudo-Canalejo, J.; Grafmüller, A.; Dimova, R.; Lipovsky, R. Patterns of Flexible Nanotubes Formed by Liquid-Ordered and Liquid-Disordered Membranes. *ACS Nano* **2016**, *10*, 463–474.
- (47) Wang, J.; Segatori, L.; Biswal, S. L. Probing the Association of Triblock Copolymers with Supported Lipid Membranes Using Microcantilevers. *Soft Matter* **2014**, *10*, 6417–6424.
- (48) Israelachvili, J. The Different Faces of Poly(Ethylene Glycol). *Proc. Natl. Acad. Sci. U. S. A.* **1997**, *94*, 8378–8379.
- (49) Hezaveh, S.; Samanta, S.; Milano, G.; Roccatano, D. Molecular Dynamics Simulation Study of Solvent Effects on Conformation and Dynamics of Polyethylene Oxide and Polypropylene Oxide Chains in Water and in Common Organic Solvents. *J. Chem. Phys.* **2012**, *136*, 124901.
- (50) Jin, H.; Wang, W.; Chang, H.; Shen, Y.; Yu, Z.; Tian, Y.; Yu, Y.; Gong, J. Effects of Salt-Controlled Self-Assembly of Triblock Copolymers F68 on Interaction Forces between Oil Drops in Aqueous Solution. *Langmuir* **2017**, *33*, 14548–14555.
- (51) Jain, N. J.; Aswal, V. K.; Goyal, P. S.; Bahadur, P. Salt Induced Micellization and Micelle Structures of PEO/PPO/PEO Block Copolymers in Aqueous Solution. *Colloids Surf., A* **2000**, *173*, 85–94.
- (52) Nozary, S.; Modarress, H.; Eliassi, A. Cloud-Point Measurements for Salt + Poly(Ethylene Glycol) + Water Systems by Viscometry and Laser Beam Scattering Methods. *J. Appl. Polym. Sci.* **2003**, *89*, 1983–1990.
- (53) Florin, E.; Kjellander, R.; Eriksson, J. C. Salt Effects on the Cloud Point of the Poly(Ethylene Oxide)+ Water System. *J. Chem. Soc., Faraday Trans. 1* **1984**, *80*, 2889.
- (54) Wu, G.; Lee, K. Y. C. Interaction of Poloxamers with Liposomes: An Isothermal Titration Calorimetry Study. *J. Phys. Chem. B* **2009**, *113*, 15522–15531.
- (55) Wu, G.; Khant, H. A.; Yee, K.; Lee, C. Effects of Bilayer Phases on Phospholipid-Poloxamer Interactions †. *Soft Matter* **2009**, *5*, 1496–1503.
- (56) Malhotra, R.; Valuckaite, V.; Staron, M. L.; Theccanat, T.; D'Souza, K. M.; Alverdy, J. C.; Akhter, S. A. High-Molecular-Weight Polyethylene Glycol Protects Cardiac Myocytes from Hypoxia- and Reoxygenation-Induced Cell Death and Preserves Ventricular Function. *AJP Hear. Circ. Physiol.* **2011**, *300*, H1733–H1742.
- (57) Zhang, W.; Coughlin, M. L.; Metzger, J. M.; Hackel, B. J.; Bates, F. S.; Lodge, T. P. Influence of Cholesterol and Bilayer Curvature on the Interaction of PPO–PEO Block Copolymers with Liposomes. *Langmuir* **2019**, *35*, 7231–7241.